Supporting Information:

Photophysical Dynamics of a Binuclear Cu(I)-Emitter on the fs to µs Timescale, in Solid Phase and in Solution

Table of Contents

Tab. S1: Decadic molar extinction coefficient ε (L mol^{-1} cm^{-1}) of **1** at given wavelengths in solution.

solvent	ε (L mol^{-1} cm^{-1}) at 350 nm	ε (L mol^{-1} cm^{-1}) at 250 nm
toluene	6000	17700
acetonitrile	4200	78400
dichloromethane	7000	72000

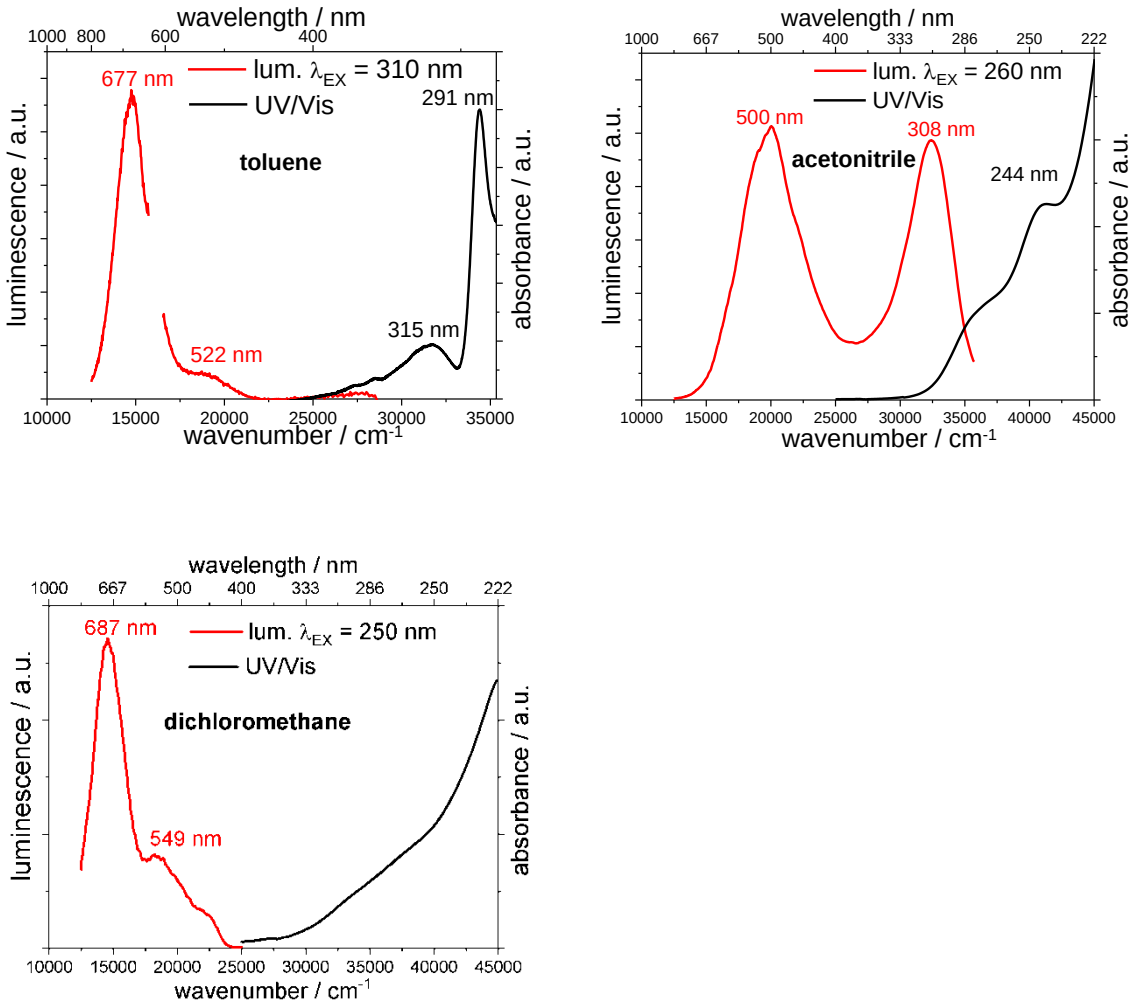

Fig. S1: Absorbance (black) and luminescence (red) spectra of **1** in toluene (9 µmol/L), acetonitrile (11 µmol/L), dichloromethane (51 µmol/L); solvent contributions subtracted (room temperature).

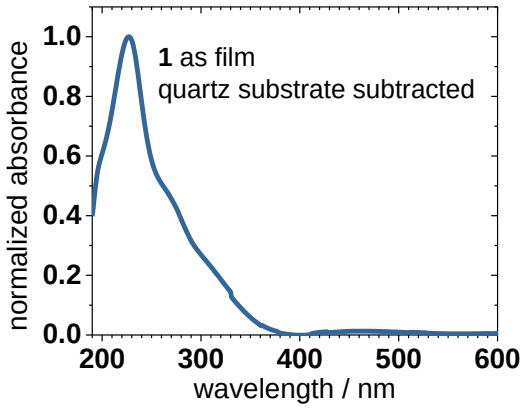

Fig. S2: Normalized static absorbance spectrum of **1** in solid state as neat film at room temperature; substrate contributions subtracted.

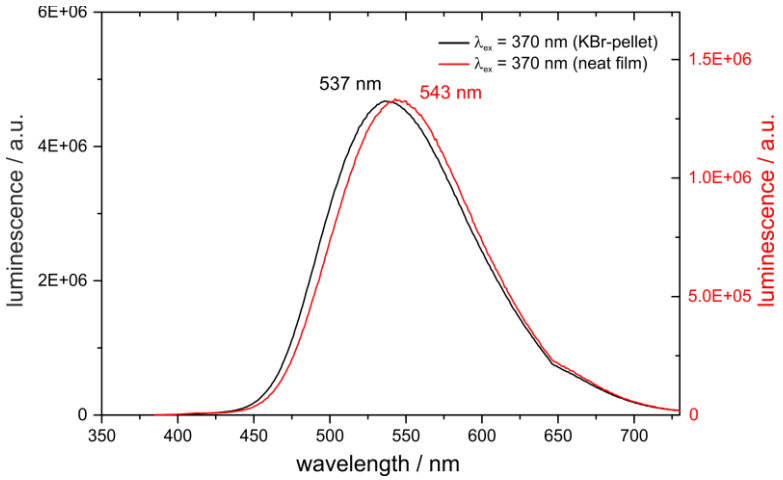

Fig. S3: Luminescence spectrum of **1** in KBr matrix (black) and luminescence spectrum of **1** as neat film (red) at room temperature.

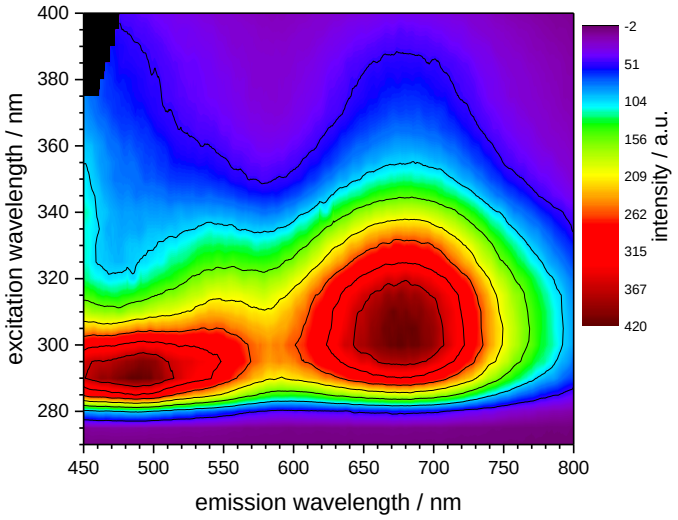

Fig. S4: Static excitation/emission spectrum of **1** in toluene solution at room temperature, concentration set to 0.02 mg/mL (14 µmol/L). Note that at high concentration used in Ref. [1] (ca. 1 mmol/L) (i) the apparent luminescence peak at 677 nm is blue-shifted to ca. 600 nm, and (ii) the excitation spectrum (for luminescence at 600 nm) is significantly red-shifted with respect to the peak at ca. 310 nm at low concentration.

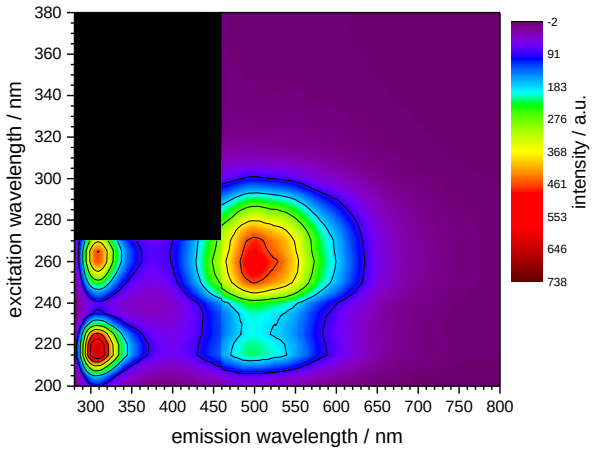

Fig. S5: Static excitation/emission spectrum of **1** in acetonitrile solution at room temperature, concentration set to 0.014 mg/mL (11 µmol/L). Note that at high concentration used in Ref. [1] (ca. 1 mmol/L) (i) the apparent luminescence peak at 500 nm is red-shifted to ca. 600 nm, and (ii) the excitation spectrum (for luminescence at 600 nm) peaks at ca. 350 nm.

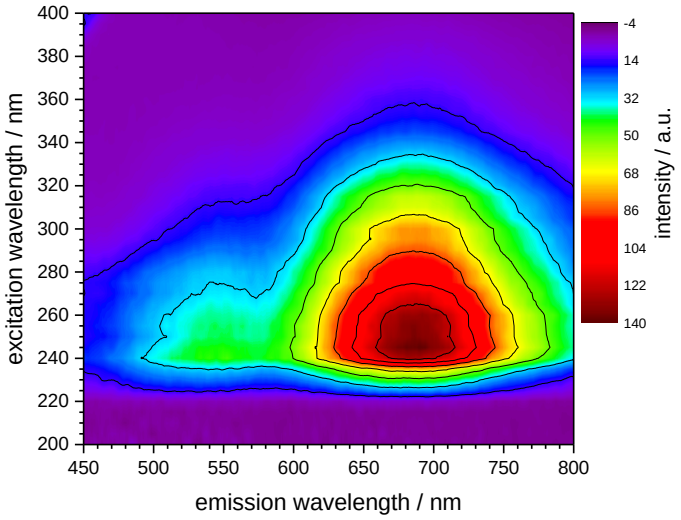

Fig. S6: Static excitation/emission spectrum of **1** in dichloromethane solution at room temperature, concentration set to 0.07 mg/mL (51 µmol/L). Note that at high concentration used in Ref. [1] (ca. 1 mmol/L) (i) the apparent luminescence peak at 685 nm is blue-shifted to ca. 600 nm, and (ii) the excitation spectrum (for luminescence at 600 nm) peaks at ca. 350 nm.

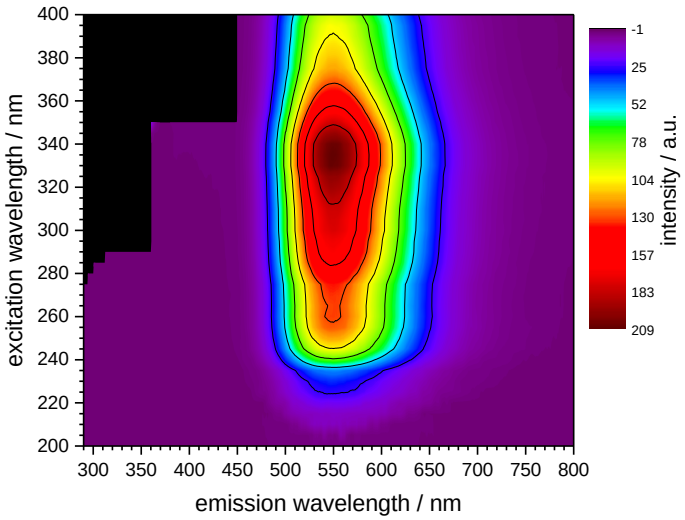

Fig. S7: Static excitation/emission spectrum of **1** as neat film at room temperature.

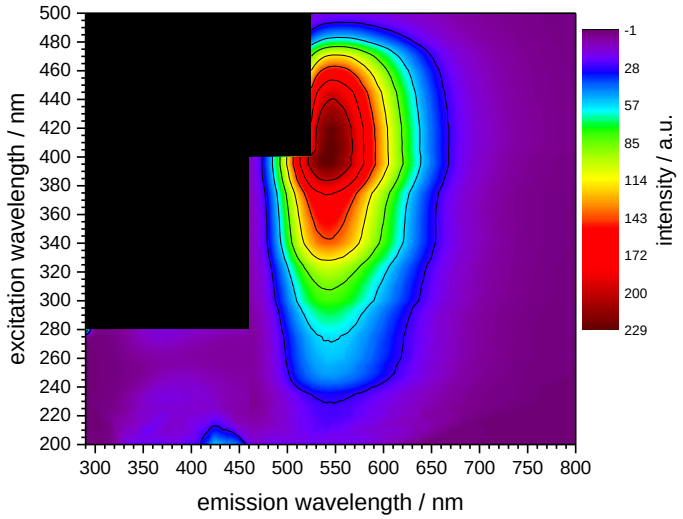

Fig. S8: Static excitation/emission spectrum of **1** as neat pellet at room temperature.

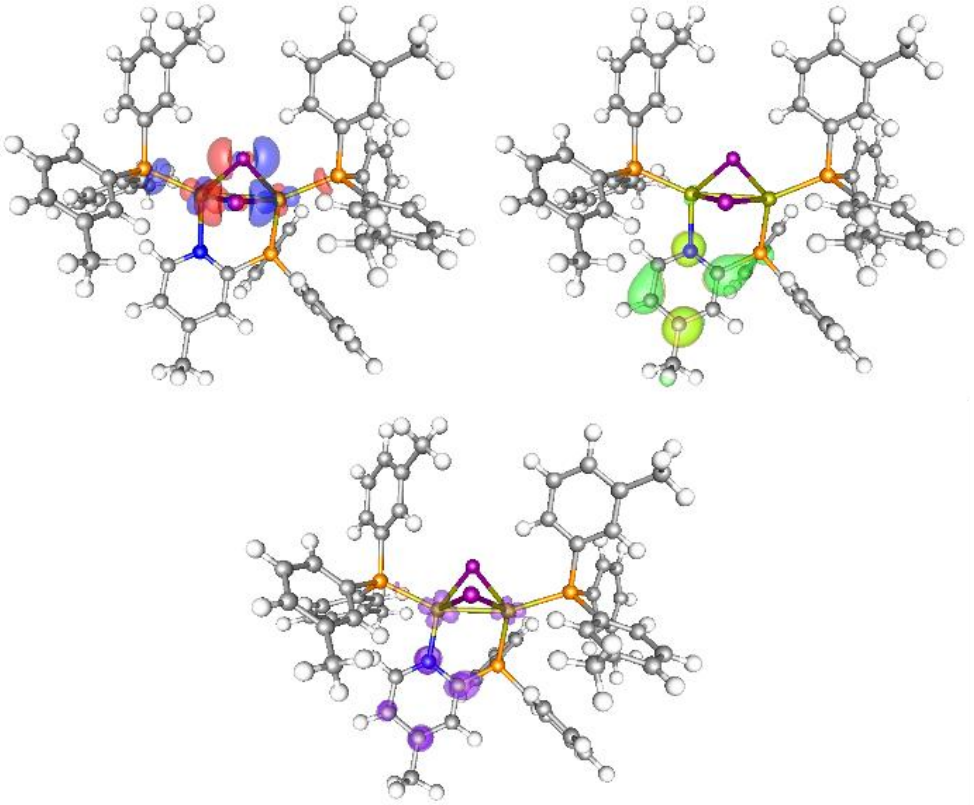

Fig. S9: Top: HOMO (left) and LUMO (right) of **1**. Bottom: Spin density in the T_1 state, calculated with DFT/B3LYP/def2-TZVP.

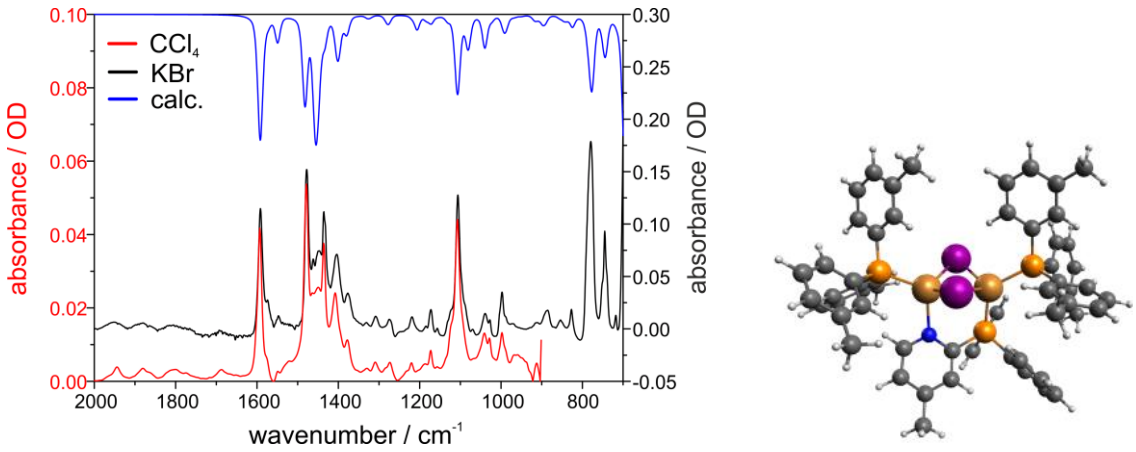

Fig. S10: Ground state FTIR spectrum of **1** in CCl_4 (red) and of **1** as KBr-pellet (black) at room temperature in comparison with calculated vibrational spectrum (blue) (S_0, DFT/B3LYP/def2-TZVP, x-axis scaled by 0.975, FWHM = 15 cm^{-1}); calculated molecular structure of **1** in the electronic ground state (right).

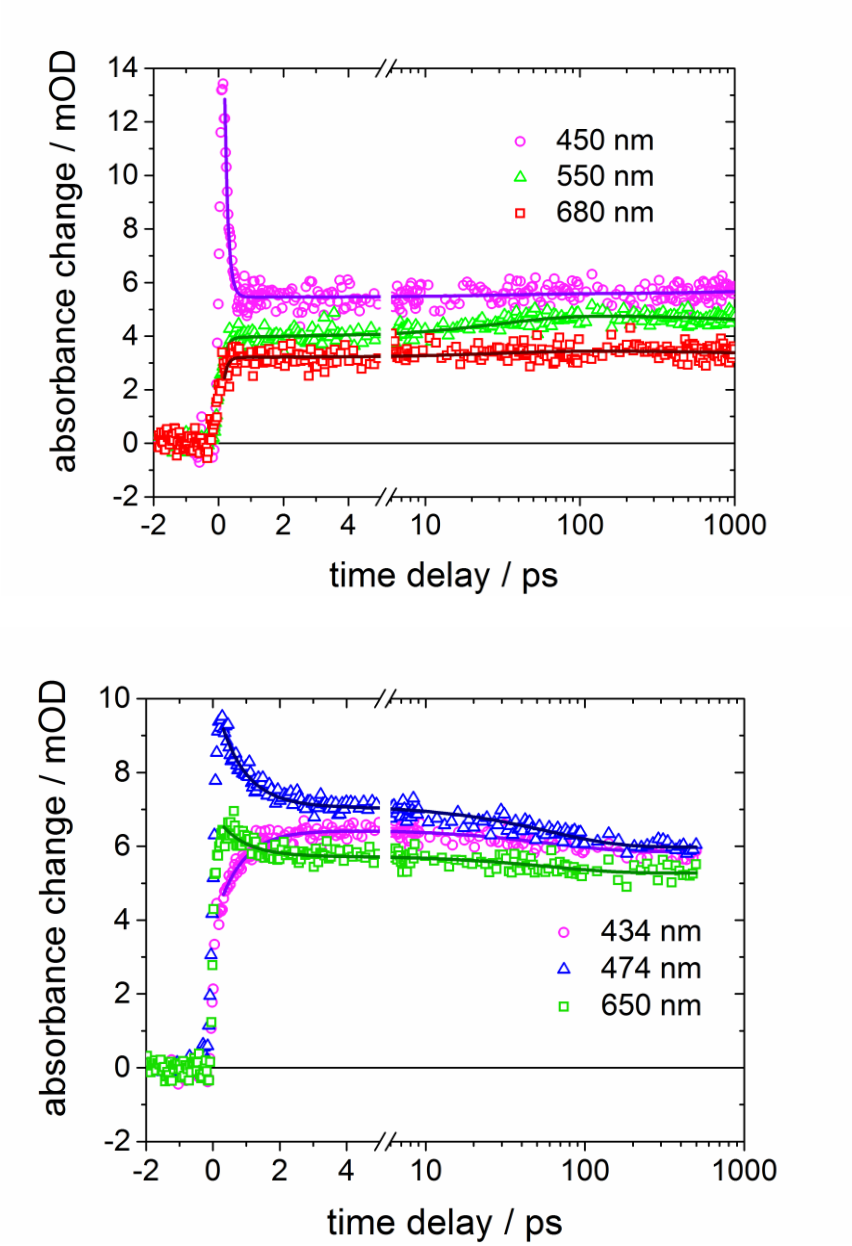

Fig. S11: Top: Selected time traces of fs transient absorption (TA) experiment on **1** in toluene solution at room temperature (excitation 350 nm) with triexponential fit (0.1, 25, 1500 ps). Bottom: Selected transients of fs-TA experiment on **1** in acetonitrile solution (excitation 350 nm) with biexponential fit (0.8, 59 ps).

Tab. S2: Luminescence lifetimes of **1** in toluene solution at room temperature.

λ_{ex} /nm	λ_{em} /nm	τ_1 /ns	A_1 /%	τ_2 /ns	A_2 /%	τ_{av} /ns
293	677	0.7	23.9	12.9	76.1	10.0

Tab. S3: Luminescence lifetimes of **1** in acetonitrile solution at room temperature.

λ_{ex} /nm	λ_{em} /nm	τ_1 /ns	A_1 /%	τ_2 /ns	A_2 /%	τ_{av} /ns
256	577	3.1	86.9	13.0	13.1	4.4
273	577	3.2	85.9	10.9	14.1	4.3

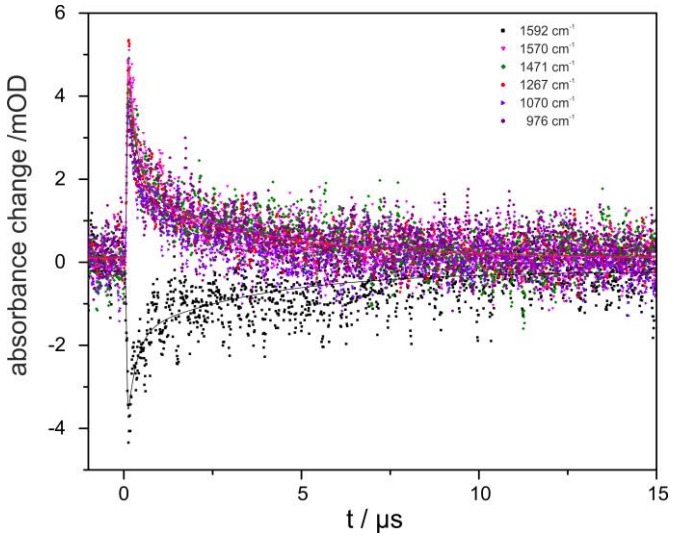

Fig. S12: Temporal evolution of step-scan FTIR absorbance changes of **1** as KBr-pellet at room temperature of 6 vibrational bands (dots) and biexponential fits (convolution with Gaussian pulse shape) (solid lines) that resulted in two decay times of τ_1 = 257 ± 14 ns and τ_2 = 3624 ± 132 ns.

Tab. S4: Characterization of vibrational modes of **1**.

$\tilde{\nu}$ /cm^{-1} ground state	$\tilde{\nu}$ /cm^{-1} excited state	**Character of the vibration**
1592		C_3-C_4 / C_5-C_6 stretching, accompanied with C-H scissoring, in the pyridine
1478	1471	C-H rocking in the tolyl moieties
1436	1427	C-H scissoring of the methyl groups of the tolyl moieties
1405		C-H scissoring in the tolyl moieties
1173	1165	C-H scissoring of tolyl and pyridine
1106		C-H scissoring of tolyl, coupled over all tolyl groups
1038		C-H twisting of the methyl group on the pyridine
998	976	Breathing of the phenyl groups
Exclusive excited state vibrations		
	1570	C-C stretching, accompanied with C-H scissoring, in the tolyl moieties
	1518	C_3-C_4 / C_5-C_6 stretching, accompanied with C-H scissoring, in the pyridine
	1267	Asymmetric N-C_2/N-C_6 stretching vibration, accompanied with C-H scissoring, in the pyridine
	1213	Breathing of the pyridine ring, accompanied with C_6-P stretching vibration

Tab. S5: Change of geometrical parameters concerning the copper – iodide core with transition from the S_0 structure to the T_1 structure, calculated with DFT/B3LYP/def2-TZVP. The numbers of the atoms are shown in the figure above.

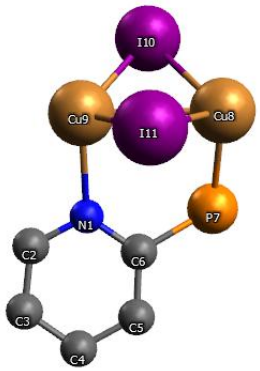

parameter	**difference**
d(N1-C6)	+0.07 Å
d(Cu8-Cu9)	-0.25 Å
d(Cu9-N1)	-0.27 Å
∠(Cu9-I10-Cu8)	-6.5°
∠(Cu9-I11-Cu8)	-6.8°

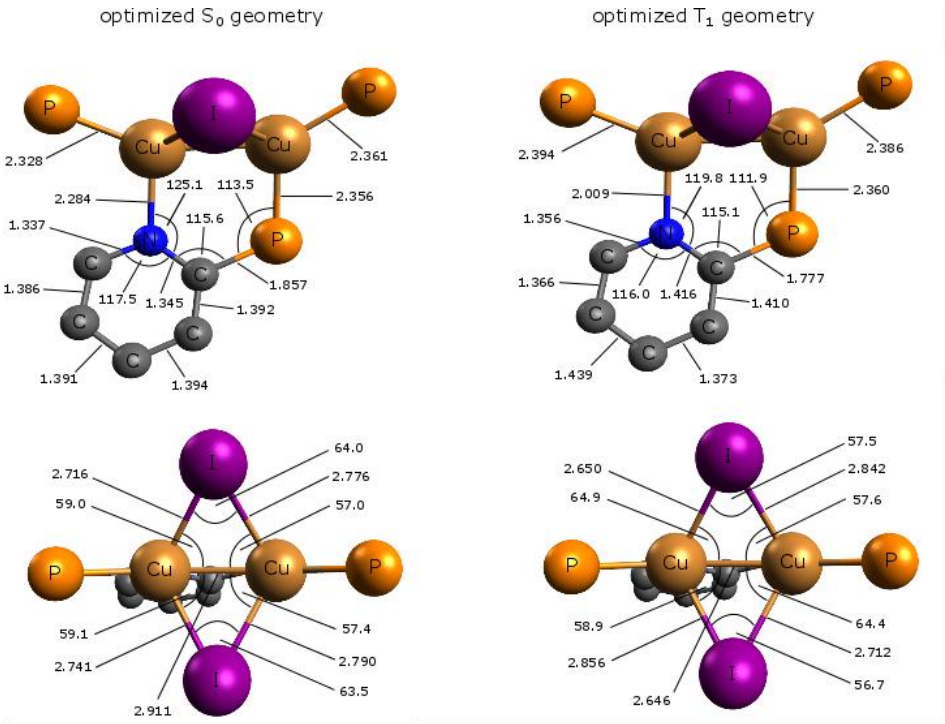

Fig. S13: Bond lengths (in Å) and angles (in °) in the central Cu_2I_2 unit in the S_0 and T_1 electronic state, calculated with DFT/B3LYP/def2-TZVP.

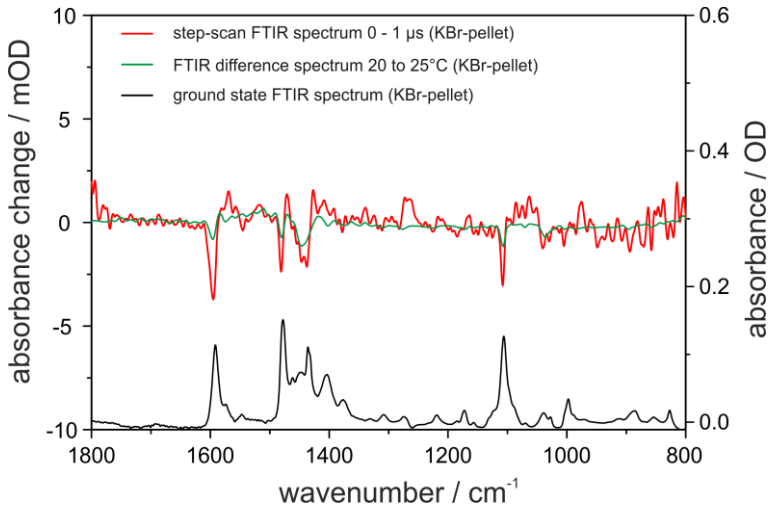

Fig. S14: Ground state FTIR spectrum of **1** as KBr-pellet (black); step-scan FTIR difference spectrum (red) in the first microsecond after excitation with 355 nm (red); change in absorbance through temperature rise of 5 K (green).

Tab. S6: Luminescence lifetimes of **1** as KBr-pellet at room temperature.

λ_{ex}/nm	λ_{em}/nm	τ_1 /µs
345	550	4.4
293	550	4.5
273	550	4.7

Tab. S7: Luminescence lifetimes of **1** as neat film at room temperature.

λ_{ex} /nm	λ_{em} /nm	τ_1 /µs	A_1 /%	τ_2 /µs	A_2 /%	τ_{av} /µs
389	550	1.03	14	4.23	86	3.8
345	550	0.76	23	3.62	77	3.0
313	550	0.69	23	3.61	77	2.9
293	550	0.63	24	3.54	76	2.8
273	550	0.61	25	3.43	75	2.7
256	550	0.56	25	3.45	75	2.7

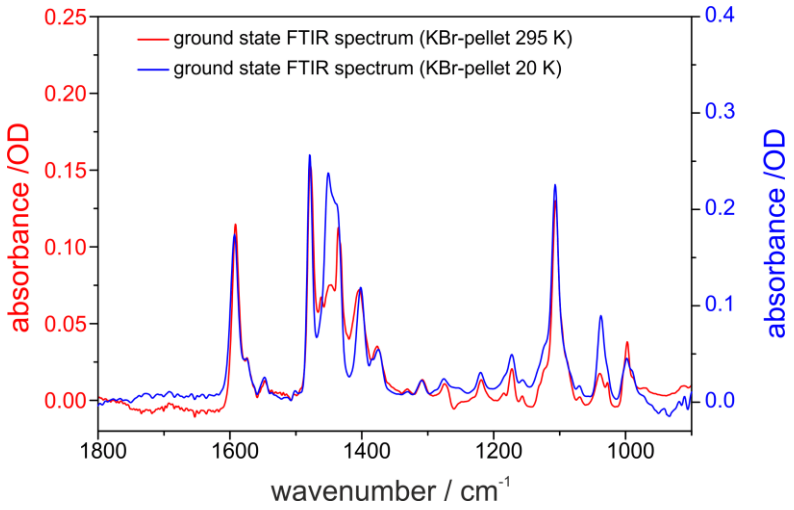

Fig. S15: Ground state FTIR spectrum of **1** as KBr-pellet at room temperature (295 K) (red) and at 20 K (blue).

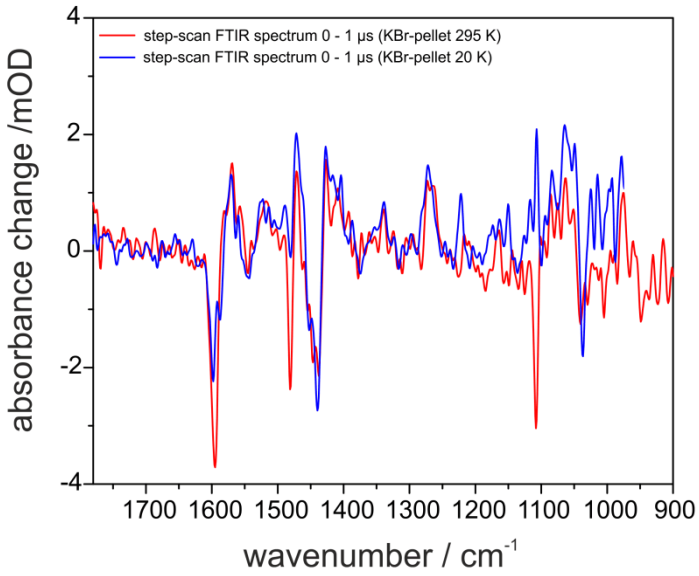

Fig. S16: Step-scan FTIR difference spectrum of **1** as KBr-pellet in the first microsecond after excitation with 355 nm, at 295 K (red) and at 20 K (blue).

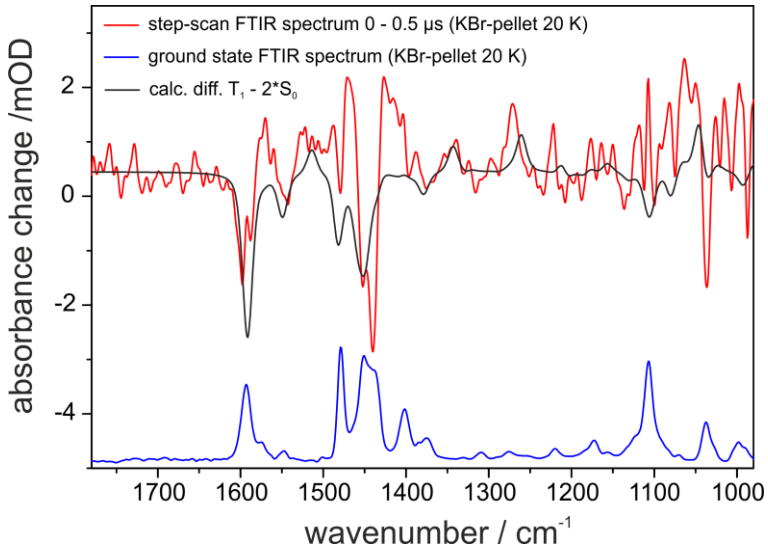

Fig. S17: Step-scan FTIR difference spectrum of **1** as KBr-pellet at 20 K in the first 500 ns after excitation with 355 nm (red); DFT calculation of T_1 state minus $2*S_0$ state (black); ground state FTIR spectrum as KBr-pellet at 20 K (blue); calculations: DFT/B3LYP/def2-TZVP, x-axis scaled by 0.975, FWHM = 15 cm^{-1}.

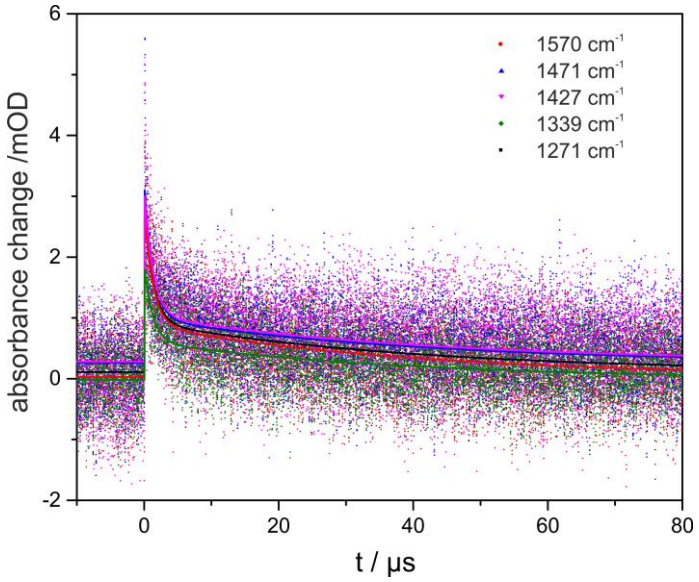

Fig. S18: Temporal evolution of step-scan FTIR absorbance changes of **1** as KBr-pellet at 20 K of 5 vibrational bands (dots) and biexponential fits (convolution with Gaussian pulse shape) (lines). $\tau_1 = 1291 \pm 49$ ns, $\tau_2 = 40 \pm 1.2$ µs.

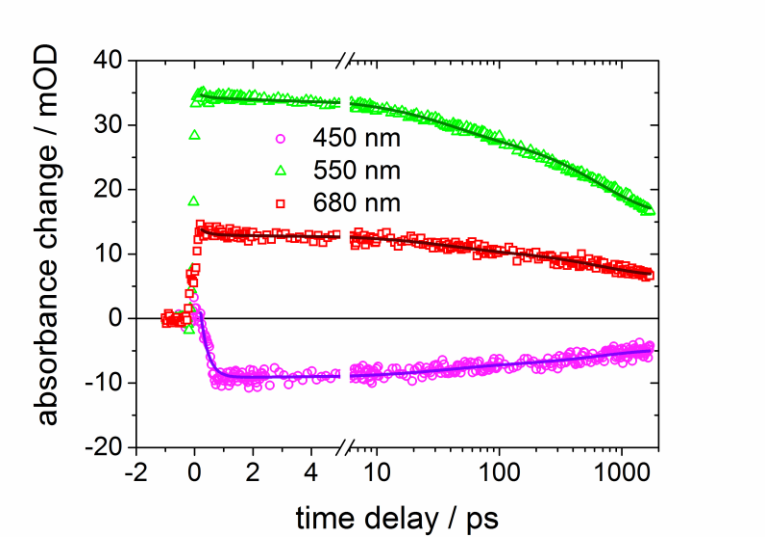

Fig. S19: Selected transients of fs-TA experiment on **1** as neat film at room temperature (excitation 350 nm) with triexponential fit (0.3, 35, 670 ps).

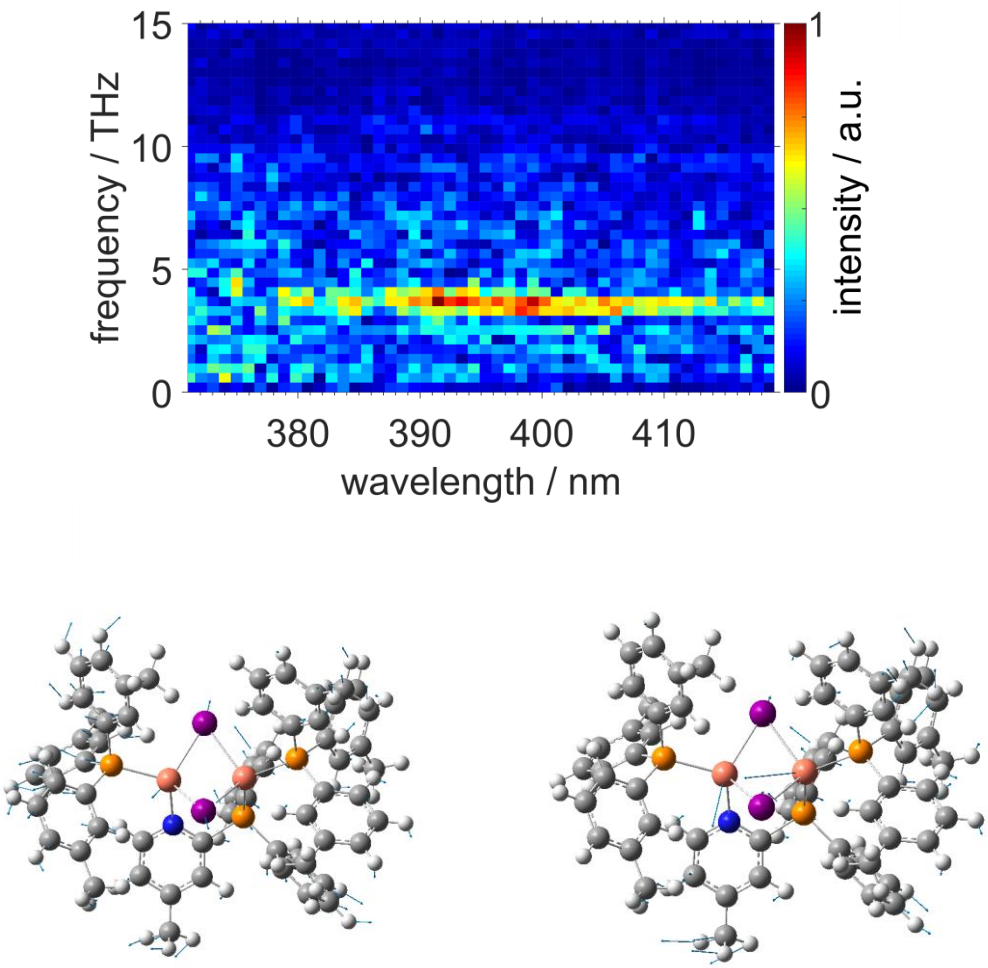

Fig. S20: Top: Fast Fourier transform (FFT) of fs-TA data of **1** in neat film at room temperature indicates coherent nuclear oscillation between ca. 390-400 nm. For more information cf. main text. Bottom: Representation of low-frequency vibrational modes in the electronic ground state of **1** (calculated by DFT) with wavenumbers (129 cm^{-1} left, 111 cm^{-1} right) close to that (115 cm^{-1}) observed after photoexcitation of **1** as neat film.

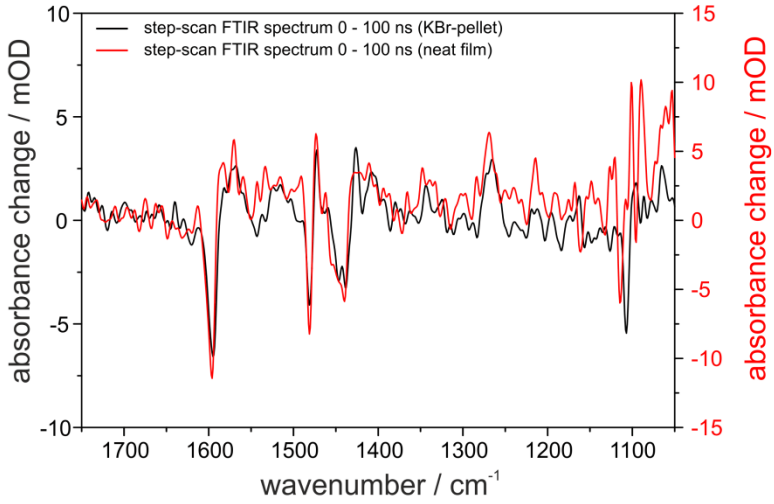

Fig. S21: Step-scan FTIR difference spectrum of **1** as KBr pellet (black) and as neat film (red) at room temperature in the first 100 ns after excitation with 355 nm.

Tab. S8: Vertical excitation energies for the S_0 geometry and corresponding oscillator strengths, calculated with TD-DFT/B3LYP/def2-TZVP.

Excited state	ΔE/eV	$\tilde{\nu}$/cm^{-1}	λ/nm	oscillator strength
S_1	2.571	20738	482	0.0012
S_2	2.867	23123	432	0.0041
S_3	2.900	23387	428	0.0116
S_4	2.959	23868	419	0.0009
S_5	3.128	25228	396	0.0028
S_6	3.248	26193	382	0.0029
S_7	3.271	26381	379	0.0021
S_8	3.284	26488	378	0.0040
S_9	3.304	26648	375	0.0166
S_{10}	3.321	26792	373	0.0033

Excited state	ΔE/eV	$\tilde{\nu}$/cm^{-1}	λ/nm	oscillator strength
T_1	2.554	20600	485	0.0058
T_2	2.770	22341	447	0.0495
T_3	2.835	22864	437	0.0216
T_4	2.946	23765	421	0.0043
T_5	3.103	25026	400	0.0247
T_6	3.154	25438	393	0.0599
T_7	3.170	25568	391	0.1029
T_8	3.226	26016	384	0.1143
T_9	3.250	26211	382	0.0268
T_{10}	3.263	26341	380	0.0160

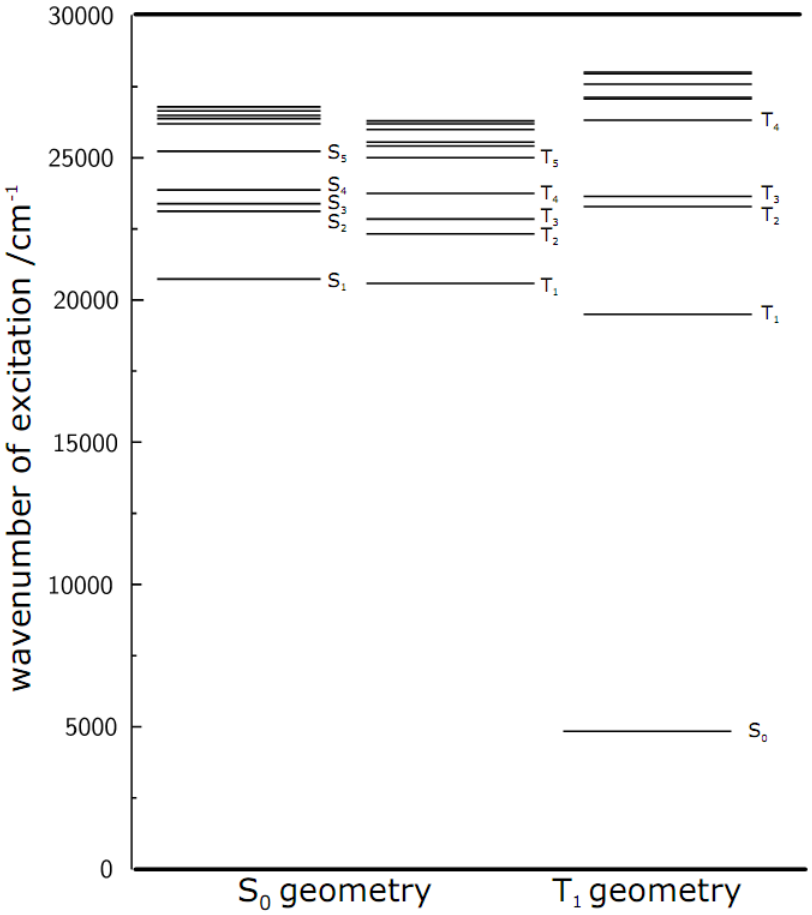

Fig. S22: Vertical excitation energies for S_0- and T_1-geometry, calculated with TD-DFT/B3LYP/def2-TZVP.

References:

[1] Wallesch, M.; Verma, A.; Flechon, C.; Flügge, H.; Zink, D. M.; Seifermann, S. M.; Navarro, J. M.; Vitova, T.; Göttlicher, J.; Steininger, R. *et al.* Towards Printed Organic Light-Emitting Devices: A Solution-Stable, Highly Soluble CuI -NHetPHOS. *Chem. Eur. J.* **2016**, *22*, 16400–16405.